Journal of Materials Chemistry B

PAPER

View Article Online
View Journal | View Issue

Cite this: J. Mater. Chem. B, 2014, 2, 4250

Solid state synthesis of carbon-encapsulated iron carbide nanoparticles and their interaction with living cells†

Valery Davydov,[a] Alexandra Rakhmanina,[a] Igor Kireev,[b] Irina Alieva,[b] Oksana Zhironkina,[b] Olga Strelkova,[b] Varvara Dianova,[b] Taraneh Djavanbakht Samani,[c] Karina Mireles,[c] L. 'Hocine Yahia,[c] Rustem Uzbekov,[de] Viatcheslav Agafonov*[f] and Valery Khabashesku‡*[g]

Superparamagnetic carbon-encapsulated iron carbide nanoparticles (NPs), Fe_7C_3@C, with unique properties, were produced from pure ferrocene by high pressure–high temperature synthesis. These NPs combine the merits of nanodiamonds and SPIONs but lack their shortcomings which limit their use for biomedical applications. Investigation of these NPs by X-ray diffraction, electron microscopy techniques, X-ray spectroscopic and magnetic measurement methods has demonstrated that this method of synthesis yields NPs with perfectly controllable physical properties. Using magnetic and subsequent fractional separation of magnetic NPs from residual carbon, the aqueous suspensions of Fe_7C_3@C NPs with an average particle size of ~25 nm were prepared. The suspensions were used for *in vitro* studies of the interaction of Fe_7C_3@C NPs with cultured mammalian cells. The dynamics of interaction of the living cells with Fe_7C_3@C was studied by optical microscopy using time-lapse video recording and also by transmission electron microscopy. Using novel highly sensitive cytotoxicity tests based on the cell proliferation assay and long-term live cell observations it was shown that the internalization of Fe_7C_3@C NPs has no cytotoxic effect on cultured cells and does not interfere with the process of their mitotic division, a fundamental property that ensures the existence of living organisms. The influence of NPs on the proliferative activity of cultured cells was not detected as well. These results indicate that the carbon capsules of Fe_7C_3@C NPs are air-tight which could offer great opportunities for future use of these superparamagnetic NPs in biology and medicine.

Received 14th November 2013
Accepted 20th April 2014

DOI: 10.1039/c3tb21599g

www.rsc.org/MaterialsB

1 Introduction

Currently, superparamagnetic NPs represent one of the most promising classes of materials because of their possible applications in various fields of biomedicine.[1–6] The ability to control magnetic properties of superparamagnetic NPs opens up a number of specific uses of these NPs in the biomedical field, and makes them unique among a wide range of non-magnetic nanostructured systems. The possibility of using such materials as intracellular markers, diagnostic probes and base platforms for the delivery of drugs and gene therapy materials and other purposes has also been actively investigated in recent years.[7–14]

To date, various physical and chemical methods have been developed for the synthesis of magnetic NPs on the basis of pure metals (Fe, Co, Ni), metal alloys, metal oxides (γ-Fe_2O_3, Fe_3O_4, $MgFeO_4$, $CoFe_2O_4$, Mn_3O_4), carbides (Fe_7C_3, Fe_3C) and other substances.[1–6,15–20]

However, direct use of these pristine NPs in biology and medicine, in general, is not feasible, because these NPs do not meet a number of specific requirements for their biomedical applications. These requirements include biocompatibility, chemical resistance and resistance to aggregation in biological media, dimensional homogeneity, and the ability to be functionalized at their surface by different types of ligands. A

[a]Institute of High Pressure Physics RAS, 142190 Troitsk, Moscow region, Russia
[b]A.N.Belozersky Institute of Physico-Chemical Biology, Moscow State University, 119992 Moscow, Russia
[c]Laboratoire d'Innovation et d'Analyse de Bioperformance École Polytechnique de Montréal, Succursale Centre-ville Montréal, Québec H3C 3A7, Canada
[d]Laboratoire Biologie Cellulaire et Microscopie Electronique, Faculté de Médecine, Université François Rabelais, 37032 Tours, France
[e]Faculty of Bioengineering and Bioinformatics, 11992, Moscow State University, Moscow, Russia
[f]GREMAN, UMR CNRS 7347, Université François Rabelais, 37200 Tours, France. E-mail: viatcheslav.agafonov@univ-tours.fr
[g]Department of Chemical and Biomolecular Engineering, University of Houston, 4800 Calhoun Rd, Houston, Texas 77204, USA. E-mail: valery@uh.edu

† Electronic supplementary information (ESI) available. See DOI: 10.1039/c3ta21599g

‡ Present address: Center for Technology Innovation, Baker Hughes Inc., Houston, TX, 77040, USA.

number of challenges to the application of superparamagnetic NPs in biomedicine can be overcome by the design of their so called "core/shell" complexes with biocompatible and durable coatings. The coatings can be of various inorganic or organic nature, depending on the specific research and application objectives. Currently, as a biocompatible coating of magnetic NPs, various surfactants, synthetic polymers, natural macromolecules, silicones, and layers of noble metals[2–6] are widely used. For example, to induce hydrophilic properties, polyethylene glycol (PEG) or polyvinyl alcohol is used for the coating of the NPs.[21–23] Other coatings, such as polyethylenimine, increase cationic surface properties.[24] Coatings of proteins and peptides help to reduce cytotoxicity and enhance the capture of the nanocomplex by the cells.[25]

Here we describe a method to produce Fe_7C_3@C NPs that combine the merits of nanodiamonds and SPIONs yet lacking their shortcomings. Like the surface of nanodiamonds, the carbon shell coating of Fe_7C_3@C NPs can be easily modified with appropriate biologically active moieties. In addition, unlike nanodiamond particles, our NPs possess magnetic properties that exceed those of SPIONs, ensuring better magnetocontrollability. We also expected that the presence of a protective carbon shell would significantly decrease toxicity typically observed for unmodified SPIONs. The cytotoxicity of NPs is a key factor limiting their use in biomedicine both at cellular and organism levels. The toxic effects are usually assayed by scoring live/dead cells, however, extremely sensitive cellular processes, such as DNA replication and cell division, can also be affected causing irreversible physiological changes (such as stem cell population homeostasis, tissue renewal, *etc.*), yet not directly leading to cell death. Therefore in cytotoxicity studies of Fe_7C_3@C NPs we used novel highly sensitive cytotoxicity tests based on proliferation assays and long-term live cell imaging in order to exclude subtle effects of the NPs on cell division.

Obviously, the practical use of such nanocomplexes requires extensive studies of their behavior in biological systems. To date, a detailed study of various aspects of biomedical use of superparamagnetic nanocomplexes was conducted essentially on only one type of NP, namely SPIONs – superparamagnetic iron oxide NPs. In a series of reviews,[2–6] the synthesis, application of protective shells, their functionalization and behavior of NPs in the biological field have been discussed in detail. Despite significant progress in the development of methods for the synthesis of nanosystems based on SPIONs, numerous studies have shown that their relatively low value of magnetization creates difficulties in the control of their magnetic behavior in a number of applications. For this reason, carbon-encapsulated superparamagnetic NPs of metals and their carbides attract increasing attention.[26,27] Significant advantages of these materials, as compared to SPIONs, for a number of biomedical applications have been clearly demonstrated in a recent paper[27] discussing the possibility of the use of carbon-encapsulated superparamagnetic FeCo@C NPs as multimodal imaging probes and cooperative therapeutic agents for tumor cells. This work suggests that because of the high value of the magnetization saturation FeCo@C NPs have higher potential than SPIONs for biomedical applications, particularly in MRI and hyperthermia.

The present work is devoted to studies of the biocompatibility and possibility of biomedical use of superparamagnetic NPs of iron carbide Fe_7C_3 encapsulated into a carbon shell. It is known, that iron carbides Fe_7C_3 and Fe_3C (cementite) are ferromagnetic with Curie temperatures of 250 and 210 °C having the magnetization saturation values of 120 emu g^{-1} and 125 emu g^{-1}, respectively, at room temperature.[28]

Given the relatively high value of the magnetization of iron carbides, the NPs with superparamagnetic cores encapsulated into a stable carbon shell, designated as Fe_7C_3@C and Fe_3C@C, appear to be very interesting for biomedical applications. Note that the presence of a carbon shell on the NPs offers great opportunities for a variety of options for further functionalization.

To date, there are several known methods for the synthesis of iron carbide NPs surrounded by a carbon shell. One of the first versions of the directed synthesis of NPs based on Fe_3C (cementite) and Fe_7C_3 phases has been the pyrolysis of a gas–vapor mixture of $Fe(CO)_5 + C_2H_4$ in argon by using high-power laser radiation.[17] The disadvantage of this method is the contamination of the product by α-Fe particles, which are toxic, as well as by iron oxide Fe_3O_4, due to the presence of oxygen in the initial reaction mixture. Recently, different methods for synthesis of encapsulated iron carbide NPs have been proposed.[19,20] However, the size of these particles was quite large, therefore they displayed ferromagnetic, but not superparamagnetic behavior. The proof-of-concept capability for synthesis of superparamagnetic encapsulated NPs Fe_7C_3@C and Fe_3C@C using ferrocene transformations induced by high pressures and high temperatures treatment (HPHTT) was demonstrated in preliminary reports.[29,30] By analogy with SPIONs, these particles were termed SCICNs (Superparamagnetic Carbon-encapsulated Iron Carbide NPs).

The objectives of the present work were (i) more detailed studies of the possibilities of the HPHTT method for the synthesis of SCICNs, namely Fe_7C_3@C, with controlled particle sizes, (ii) the development of methods for magnetic separation and size fractionation of synthesized superparamagnetic NPs, (iii) *in vitro* studies of interactions of water-dispersed Fe_7C_3@C NPs with living cultured cells, (iv) testing the cytotoxicity of the NPs and exploring their possible effect on the proliferative activity of the cells and cell division.

2 Experimental

Ferrocene (Aldrich, impurity contents less than 2%) was used as a starting material without further purification. Cold-pressed pellets of the pristine ferrocene (4.5 mm diameter and 3 mm height) were inserted into a graphite heater and then placed into a high pressure cell. High pressure high temperature treatment (HPHTT) of the samples was performed with the use of a high pressure apparatus of the "Toroid" type.[31] Details of the experimental procedure have been described in the preliminary report.[29] XRD experiments were carried out on an INEL CPS 120 diffractometer using Co $K\alpha_1$ radiation.

Microscopy characterization of the samples was carried out using a scanning electron microscope Ultra-Plus Gemini (Zeiss), and transmission electron microscopes JEM 1230 and JEOL 2100 for high resolution microscopy (HRTEM). Room temperature magnetization curves of the samples and the temperature dependence of the magnetization were measured with a quantum design physical property measurement system magnetometer. Separation of superparamagnetic NPs from products obtained as a result of HPHTT decomposition of ferrocene and preparation of an aqueous suspension of encapsulated Fe_7C_3@C NPs was carried out in several stages.

During the first stage, the samples were mechanically crushed in a ball mill. Further dispersion of the particles was carried out by using the ultrasonic bath for 48 hours in a 35% solution of hydrogen peroxide. At the final stage of processing, the magnetic NPs were isolated from the total solution by magnetic separation, washed 3 times with distilled water and then dried for 24 hours. Subsequent fractional separation of NPs and their aggregates was carried out by centrifugation of the obtained powder mixture in three-layer aqueous solutions of sucrose of different densities (30, 50 and 70% of sucrose) for 10 min at an acceleration of 1000 rpm. After centrifugation, the contents of the middle layer were selected from the separating capsule and then washed and dried. Size distribution in the separated fraction of NPs was measured by SEM and TEM. The structure and chemical composition of the surface layer of the obtained NPs were examined by XPS (VG ESCALAB 3 MK II, with an Mg Kα radiation source ($h\nu = 1253.6$ eV, and an instrument resolution of 0.7 eV)). At the same time, the magnetic properties of the selected fraction of superparamagnetic NPs were redetermined. The selected NPs were then dispersed in water using ultrasonication for 10 minutes. Different concentrations of water suspensions of Fe_7C_3@C NPs were prepared for biological research.

Biological tests, conducted in the current study, were primarily aimed at the evaluation of cytotoxic effects of water-based dispersions of non-modified nanocomplexes of Fe_7C_3@C superparamagnetic NPs on cultured mammalian cells of various origins (human transformed cell lines and a pig embryonic cell). Since similar investigations have not yet been conducted with such NPs, several types of sensitive cytotoxicity tests were performed including the NP internalization dynamics *in vitro*, mitotic activity measurements, DNA replication, and overall proliferative activity of cellular population upon prolonged cultivation in the presence of high concentrations of NPs in culture media.

Cytotoxicity tests were performed on pig kidney epithelial cells (PK). PK cells (kindly provided by Russian collection of cell lines, St. Petersburg) were cultured in DMEM culture medium (Sigma, USA) supplemented with 10% fetal calf serum (HyClone, USA) and antibiotic–antimycotic (Sigma, USA). For microscopy experiments, cells were placed on coverslips and incubated with various concentrations of Fe_7C_3@C NPs (from 5 to 100 μg ml^{-1}). 20 μg ml^{-1} was found to be an optimal concentration for easy particle detection by light and electron microscopy while MNP agglomerates did not significantly interfere with sectioning and imaging.

For live imaging, PK cells were placed on glass-bottomed Petri dishes (LabTek, USA) at a density of 10^5 cells per ml and incubated with Fe_7C_3@C NPs for 24 h. Cell observation was performed in an environmental chamber kept at 37 °C and under 5% CO_2. The chamber was mounted on an Olympus IX70 inverted microscope equipped with a CCD-camera Orca-RT + (Hamamatsu, Japan) and controlled by Micromanager 1.4 software.[32] Illumination conditions (ND filters, lamp voltage, and exposure time) were set to minimize phototoxicity. Image sequences were analyzed and time-lapse movies of cells loaded with SCICNS were assembled using ImageJ software.[33,34] Images were taken every 10 min for 72 h for long recording or every 1 min during short recording.

For further TEM experiments, PK cells were washed several times with fresh pre-warmed media to remove free particles, fixed in 2.5% glutaraldehyde in 100 mM phosphate buffer (pH 7.4) for 2 hours with subsequent post-fixation in 1% OsO_4 and embedding in Epon (Sigma, USA). Serial ultrathin sections (70 nm) were prepared using a Leica ultramicrotome and observed using a JEM 1011 (JEOL, Japan) at 100 kV.

3 Results

3.1 Structural characterization of Fe_7C_3@C NPs

The X-ray diffraction (XRD) pattern and TEM images of the sample obtained by heat treatment of ferrocene at 8.0 GPa and 560 °C are shown in Fig. 1 and 2, respectively. In the XRD pattern, shown in Fig. 1, the diffraction line at $2\Theta = 30.4°$ corresponds to the (002) reflection of graphite-like materials, which represent a packing of graphene layers. The group of reflections in the angular range of 44–65° mainly belongs to those of the crystalline phase of iron carbide. The latter was indexed with the hexagonal unit cell (with the parameters $a =$ 6.85 (1) and $c = 4.53$ (1) Å) corresponding to a space group $P6_3mc$ (isostructural to Ru_7B_3).[35] The substantial background level observed in the low-angle region of the diffractogram is due to

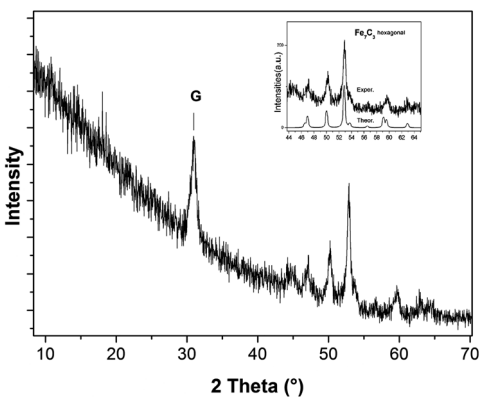

Fig. 1 XRD pattern of the sample obtained by thermal treatment of ferrocene at 8.0 GPa and 560 °C. The diffraction peak corresponding to graphitic-like carbon states is marked by G. The inset shows the experimental and simulated XRD patterns of the hexagonal phase of Fe_7C_3.

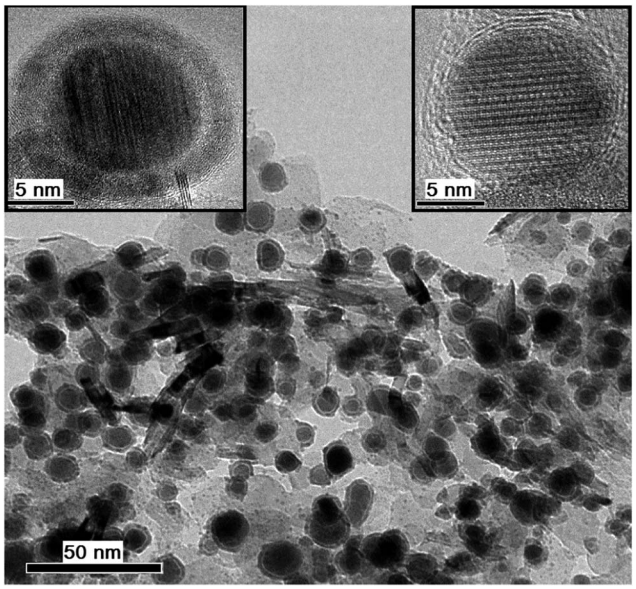

Fig. 2 TEM image of the sample obtained by thermal treatment of ferrocene at 8.0 GPa and 560 °C. The top right inset shows the HRTEM image of NPs coated with preferentially ordered carbon layers accumulated on the surface of the Fe_7C_3 core. The top left inset shows the HRTEM image of NPs coated with predominantly amorphous carbon.

the presence of an appreciable content of disordered carbon in the sample.

This interpretation of the X-ray data is consistent with the results of electron microscopic studies of the sample. An overview of a TEM image presented in Fig. 2 clearly shows that the analyzed sample represents individual NPs dispersed in a somewhat poorly ordered matrix. The NPs exhibit very distinguishable inner cores and outer shells, and show mostly quasi-spherical shapes with the sizes ranging from 10 to 30 nm. HRTEM images of the individual NPs, shown in Fig. 2 insets, suggest that the cores of the particles have an ordered crystalline structure corresponding to iron carbide Fe_7C_3. It was concluded that the surface carbon shell is formed by ordered layers built from sp^2 carbon states which characterize onion-like graphitic NPs,[36] and also by certain quantity of disordered carbon mainly representing the sp^3 carbon state. The ratio of the ordered and disordered carbon fractions in the surface layers is not constant and slightly changes from one nanoparticle to another. Regarding the structure of carbon layers in the Fe_7C_3@C NPs obtained at 8 GPa and 560 °C, it should be noted that at this temperature the system retains some amounts of hydrogen. The hydrogen atoms will interact with the surface carbon atoms having free dangling bonds. As a result of such an interaction, a certain amount of carbon on the surface will become covalently bonded to hydrogen. Therefore, the surface of outer layers of Fe_7C_3@C NPs can be considered to some extent as hydrogen terminated.

Through magnetic and fractional separations described in the Experimental section, different average size fractions of Fe_7C_3@C have been isolated in pure form. Fig. 3 (left) shows the SEM image of the conglomerate of separated NPs as well as size distributions of the NPs and their inner cores obtained by TEM measurements (Fig. 3a and b). The presented data indicate that the isolated NPs are sufficiently uniform, with the average sizes of the outer part of NPs and their magnetic cores being 25 and 16 nm, respectively.

The information on surface atomic bonding in the selected NPs was obtained from the XPS data. Fig. 4 shows the high-resolution XPS C 1s spectrum curve-fitted with five components.

Analysis of these data leads to the following attribution of the observed components. The peak at 284 eV is due to the sp^2 C–C bonding (note that this peak may also contain some contribution from the iron carbide's carbon). The peak at 285 eV is due to the sp^3 C–C bonding. The peaks at 286.3 eV, 287.5 eV and 289 eV correspond to carbons of the C–O, C═O and COOH units, respectively. These peaks indicate the partial oxidation of the sample surface in the process of its treatment by hydrogen peroxide. However, the presence of these groups on the surface of NPs could play a positive role in aiding the stability of the solution by preventing aggregation of NPs.

3.2 Magnetic properties of Fe_7C_3@C NPs

Experimental detection of superparamagnetic states of magnetic NPs is based on studies of their magnetization curves[1–3,37] and temperature dependence of magnetization measured upon cooling in a zero magnetic field (Zero-Field Cooling – ZFC) and a non-zero magnetic field (Field Cooling – FC).[1–3,38,39]

Fig. 5a presents magnetization curves (M *vs.* H) obtained at room temperature for the as-prepared product of HPHTT of ferrocene and for the separated fraction of Fe_7C_3@C.

The curves show typical superparamagnetic behavior for both studied materials, characterized by the absence of the magnetic hysteresis loop.[1–3,37] The difference between the two curves is associated with a higher value of magnetic saturation of separated fraction of Fe_7C_3@C, 54 emu g^{-1}, compared to 20 emu g^{-1} for the as-prepared sample. Obviously, this difference can be explained by a higher content of superparamagnetic carbide components in the product which is enriched through the magnetic separation procedure.

The curves of temperature dependence of magnetization, recorded for an as-prepared sample upon cooling in a zero magnetic field (ZFC) and a nonzero magnetic field (FC) (Fig. 5b), confirm the superparamagnetic nature of the Fe_7C_3@C NPs. According to the data shown in Fig. 5b, the discrepancy between the temperature dependence of $M_{FC(T)}$ and $M_{ZFC(T)}$, referred to as "the irreversibility point",[38] occurs in the product at $T_{irr} = 300$ K, which is situated below the temperature of the human body, $T = 310$ K. The position of the maximum (T_{max}) on the $M_{ZFC(T)}$ curve corresponds to a temperature of $T = 250$ K. In real nanosystems T_{max} is often identified with the average blocking temperature of these systems while the value of T_{irr} can be identified with the blocking temperature of NPs of maximum size.[1]

Thus, the magnetic characterization, carried out in this work, shows that the as-produced Fe_7C_3@C NPs, resulting from HPHTT of ferrocene, as well as the separated NPs both

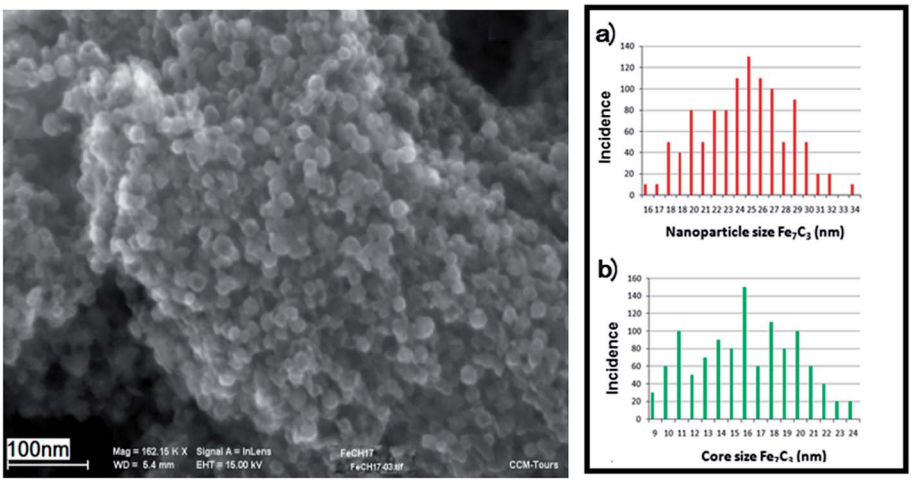

Fig. 3 SEM image of separated Fe_7C_3@C NPs (left), and dispersion diagrams (right) of the outer sizes of the NPs (a) and the sizes of their magnetic cores (b).

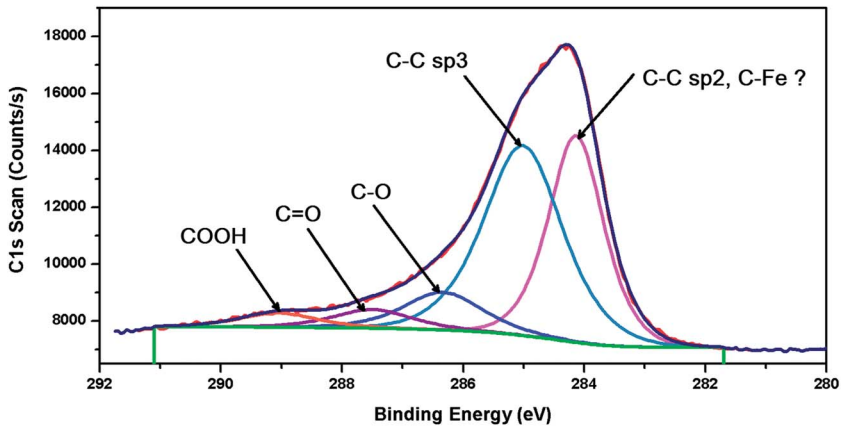

Fig. 4 High resolution XPS C 1s carbon peak observed for the Fe_7C_3@C sample.

represent truly superparamagnetic materials. However, for biological tests we have selected only the medium size fraction of Fe_7C_3@C NPs which are more homogeneous in composition.

3.3 Biological properties of Fe_7C_3@C NPs

3.3.1 *In vitro* studies of Fe_7C_3@C NP interactions with cells. In this study we have investigated the dynamics of internalization of 25 nm diameter Fe_7C_3@C NPs into pig kidney (PK) epithelial cells. These cells were selected for analysis of their interaction with the NPs since they are not specialized for phagocytosis. Our choice is based on the fact that the future targets in humans will be located in the similar type of cells. In our opinion, the phagocyte cells usually used in similar experiments are not suitable for our purposes since these cells easily absorb any external particles independent of their nature.

PK cells (kindly provided by Russian Collection of cell lines, St. Petersburg) were cultured in DMEM culture media (Sigma, USA) supplemented with 10% fetal calf serum (HyClone, USA) and antibiotic–antimycotic (100 units per ml penicillin G, 100 μg ml^{-1} streptomycin sulfate and 0.25 μg ml^{-1} amphotericin B) (Sigma, USA). For microscopic experiments cells were plated onto cover slips at a concentration of 10 000 cells per cm^2 and grown for 48 h to reach 50% confluence before the addition of various concentrations of Fe_7C_3@C NPs.

Kinetics of cell interaction with Fe_7C_3@C was studied by TEM on serial ultrathin sections, and also by optical microscopy using time lapse video recording of living cells. Quantitative characteristics of Fe_7C_3@C penetration into the cells are shown in Table 1.

TEM analysis showed that Fe_7C_3@C (Fig. 6a–c) existed in the culture media not as individual NPs but as agglomerates of various sizes (from tens to hundreds of Fe_7C_3@C particles). Several stages of Fe_7C_3@C–cell interactions have been observed. (1) At first, Fe_7C_3@C accumulate on the cell surface (Fig. 6a, Table 1). This type of interaction was detected already after 15 min of incubation of cells in the presence of Fe_7C_3@C NPs. (2) At the second stage (15–30 min), the agglomerates were found to be associated with the plasma membrane invaginations, and Fe_7C_3@C NPs during this phase started to be covered by the

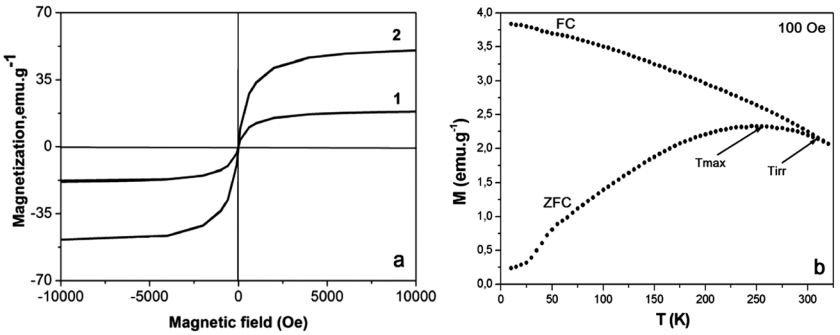

Fig. 5 The curves of magnetization *versus* the applied field obtained at room temperature for the as-prepared sample (1) and separated fraction of Fe_7C_3@C NPs (2) (a). The curves of zero field and field cooled magnetization (M_{ZFC} and M_{FC}) *versus* temperature (from 5 to 325 K) (b).

Table 1 Statistical analysis of cell–Fe_7C_3@C NP interactions[a]

Time duration of cell incubation	Cells without contact with Fe_7C_3@C, %	Contact of the cell membrane with Fe_7C_3@C, %	Invagination of the cell membrane in the place of contact with Fe_7C_3@C, %	Fe_7C_3@C into the cell, %
15 min Fe_7C_3@C (61)	80.3 (49)	16.4 (10)	3.3 (2)	0 (0)
30 min Fe_7C_3@C (64)	62.5 (40)	26.6 (17)	9.4 (6)	1.6 (1)
60 min Fe_7C_3@C (65)	44.6 (29)	26.2 (17)	10.7 (7)	18.5 (12)
120 min Fe_7C_3@C (51)	25.5 (13)	11.8 (6)	27.4 (14)	35.3 (18)

[a] Numbers given in parentheses: the first column – number of cells studied, other columns – number of cells found under given conditions.

membrane's lamellipodia (Fig. 6b and Table 1). (3) Starting from 30 min, and more often after 60 and 120 min of incubation, the Fe_7C_3@C agglomerates appear inside the cells (Fig. 6c and Table 1).

Since Fe_7C_3@C agglomerates were dispersed through the whole volume of cell culture media, the cell–Fe_7C_3@C interaction process has progressively continued during a whole period of the experiment, so we could observe all stages of interactions simultaneously in different cells, although, the ratio of different morphological types has changed with time (see Table 1).

A prolonged incubation of the cells with Fe_7C_3@C NPs (6 h or longer) led to formation of rather large Fe_7C_3@C agglomerates inside the cell cytoplasm. However, the penetration of NPs into the cell nucleus has never been observed (Fig. 6d–f). The maximum cellular uptake of Fe_7C_3@C NPs was approximately estimated using an optical microscope method and found to take place during between 12 and 48 hours incubation time when the cytoplasm became filled with slightly aggregated Fe_7C_3@C NPs, while the cells still maintained normal morphology. Simultaneously, the overall concentration of Fe_7C_3@C NPs per cell has increased with the incubation time reaching a maximum at 24 hours when all aggregates precipitated at the bottom from solution (Fig. 6d–f).

Three types of arrangements for NP agglomerates have been observed in the cell by TEM: agglomerates of particles that can be either completely surrounded by membranes, partially covered by a membrane (Fig. 6e) or be positioned freely in the cell cytoplasm (Fig. 6c).

Upon internalization and fusion of endosomes, larger agglomerates were found to be formed inside the cells. Fe_7C_3@C agglomerates also precipitated onto a cell-free surface of a cover slip and were later internalized by nearby cells during their spreading or crawling. This process was studied using live cell imaging. Results of live observations showed that cells actively capture NP agglomerates disposed on the surface of the cultivation substrate. In this case the cells were able to separate large agglomerates into smaller parts (Fig. 7). Absorbed NP agglomerates moved inside the cells at a considerable distance in the direction from the cell surface to the center of the cell. The mechanism of this movement is not yet fully understood and will be studied in detail later. Active modification of the leading edge of the cell, the formation of lamellipodia and filopodia as well as active endocytosis indicated the absence of any significant effect of the NP presence on the cell surface or inside the cell on its physiological state.

3.3.2 The effect of Fe_7C_3@C NPs on cell division. Time-lapse imaging also shows that the uptake of Fe_7C_3@C NPs does not interfere with the cell cycle progression. Live cell imaging clearly demonstrates that the cells loaded with NPs successfully enter and complete mitosis at the rate comparable to that of non-treated cells (Fig. 8, see the ESI video recording 2†). The time duration of mitosis and morphological features of the cells at different mitotic stages, including spindle size and its overall architecture, the chromosome segregation process and cytokinesis, were not affected by the presence of large numbers of Fe_7C_3@C NPs. These agglomerates moved chaotically in the cytoplasm outside the mitotic spindle and were randomly

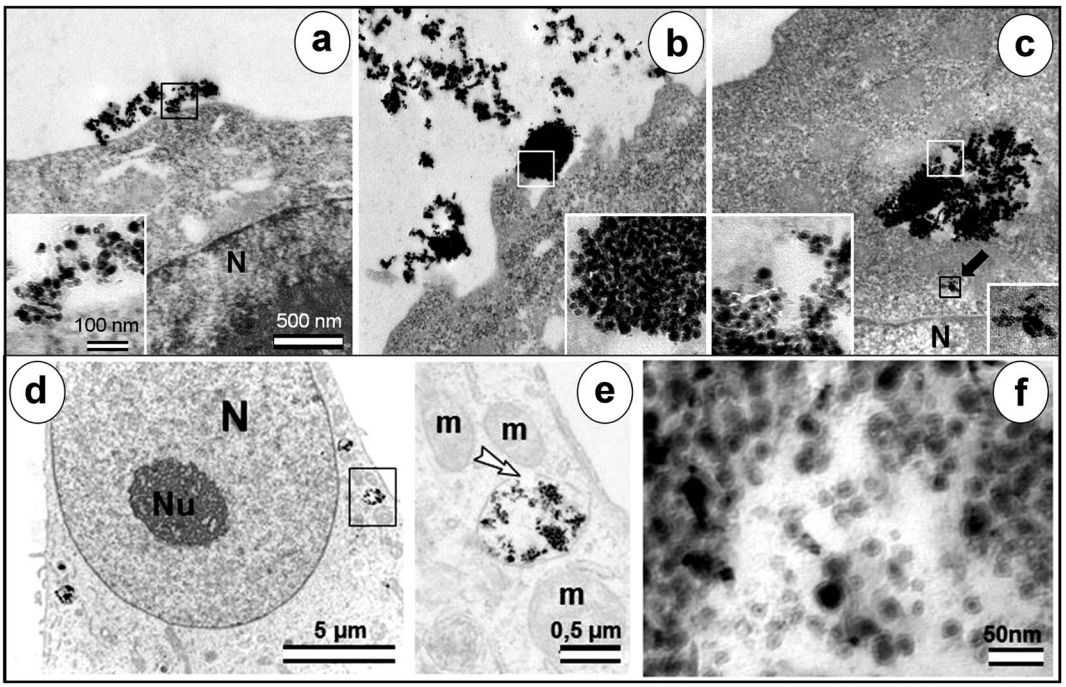

Fig. 6 TEM images of ultrathin sections cut in the direction perpendicular to the cell cultivation substrate to represent three stages of Fe_7C_3@C NP–cell interactions (a–c) and Fe_7C_3@C NP distribution in the cytoplasm of PK cells, $t = 24$ h (d–f). Contact of Fe_7C_3@C NPs with the cell surface; the inset shows a high magnification image of the selected region; $t = 30$ min (after addition of Fe_7C_3@C NPs to the cell culture medium) (a). Cell membrane invagination – the beginning of endocytosis; the inset shows the high magnification image of the selected region; $t = 30$ min, arrowheads show two membrane's lamellipodia, which cover a cluster of NPs (b). Fe_7C_3@C agglomerates inside the cell, $t = 60$ min. The large inset shows a high magnification image of the part of a big cluster surrounded by the membrane, the small inset (pointed at by an arrow) shows a small cluster without the membrane around it. N designates the cell nucleus. The scale bar for all low magnification pictures is 500 nm, for the insets – 100 nm (c). General view of the cell with the Fe_7C_3@C agglomerates incorporated into the cytoplasm, while Fe_7C_3@C NPs are missing in the nucleus (d). Enlarged region of the cell cytoplasm with the vesicle containing Fe_7C_3@C NPs. The arrow shows that the cell membrane is not continuous (e). High magnification image of the Fe_7C_3@C agglomerate in the cell, where the average diameter of an individual particle is near 25 nm. N – nucleus, Nu – nucleolus, m – mitochondria (f).

distributed between two daughter cells upon cytokinesis (video recording 2 in the ESI†). These observations indicate that the presence of Fe_7C_3@C agglomerates in the cytoplasm of dividing cells does not interfere with the process of mitotic division.

3.3.3 The effect of Fe_7C_3@C NPs on DNA synthesis. Traditional cytotoxicity tests used for the analysis of NP toxicity such as MTT, live/dead cell discrimination, *etc.* display rather low sensitivity as they score dead *versus* live cells, while toxic effects of NPs may affect cellular physiology in more subtle ways without causing cell death. For example, activation of cell cycle checkpoints prevents cellular proliferation while cells remain alive for a long time. In this respect, various cell proliferation assays are believed to be most efficient. In this study we studied the effect of Fe_7C_3@C NPs on DNA synthesis using a Click-IT HCS proliferation kit (Invitrogen, USA).

Cells incubated with or without Fe_7C_3@C for 24–48 h were labelled with a 10 μM EdU DNA synthesis precursor for 15 min, then fixed and analyzed using a fluorescence microscope Ti-E (Nikon, Japan). EdU-positive cells as well as mitotic and apoptotic cells were counted in order to evaluate Fe_7C_3@C NP cytotoxicity. Statistical analysis was performed using Excel spreadsheet software. We found that a fraction of cells in the synthetic phase of the cell cycle (S-stage) did not display statistically significant changes between control (38%, $n = 296$) and Fe_7C_3@C NP loaded (39%, $n = 182$) cell populations. Moreover, even cells heavily loaded with Fe_7C_3@C NPs are capable of DNA synthesis. Thus, a microscopy based cell proliferation assay showed that the DNA synthesis precursor EdU incorporated after 24 h incubation with Fe_7C_3@C NPs was not affected by accumulation of NPs.

3.3.4 The effect of Fe_7C_3@C NPs on cell viability and mitotic activity. Upon prolonged cultivation of PK cells with Fe_7C_3@C NPs (three consecutive passages within 10 days) we analyzed the cellular proliferation rate and cell viability. It was found that these parameters of cell population did not differ between control and Fe_7C_3@C NP-loaded samples since we did not observe any noticeable cellular death above the control level.

The mitotic index at the beginning of the experiment before adding Fe_7C_3@C NPs to cell culture medium was $4.1 \pm 0.46\%$, while after 72 h of incubation with Fe_7C_3@C NPs at a concentration of 20 μg ml^{-1} the mitotic index was $4.3 \pm 0.77\%$. Nearly 500 cells were analyzed for each point, and 4 independent measurements were taken.

We also did not notice any increase in the amount of cells subject to apoptotic degradation as assayed by microscopic analysis of nuclear morphology. In the control samples this

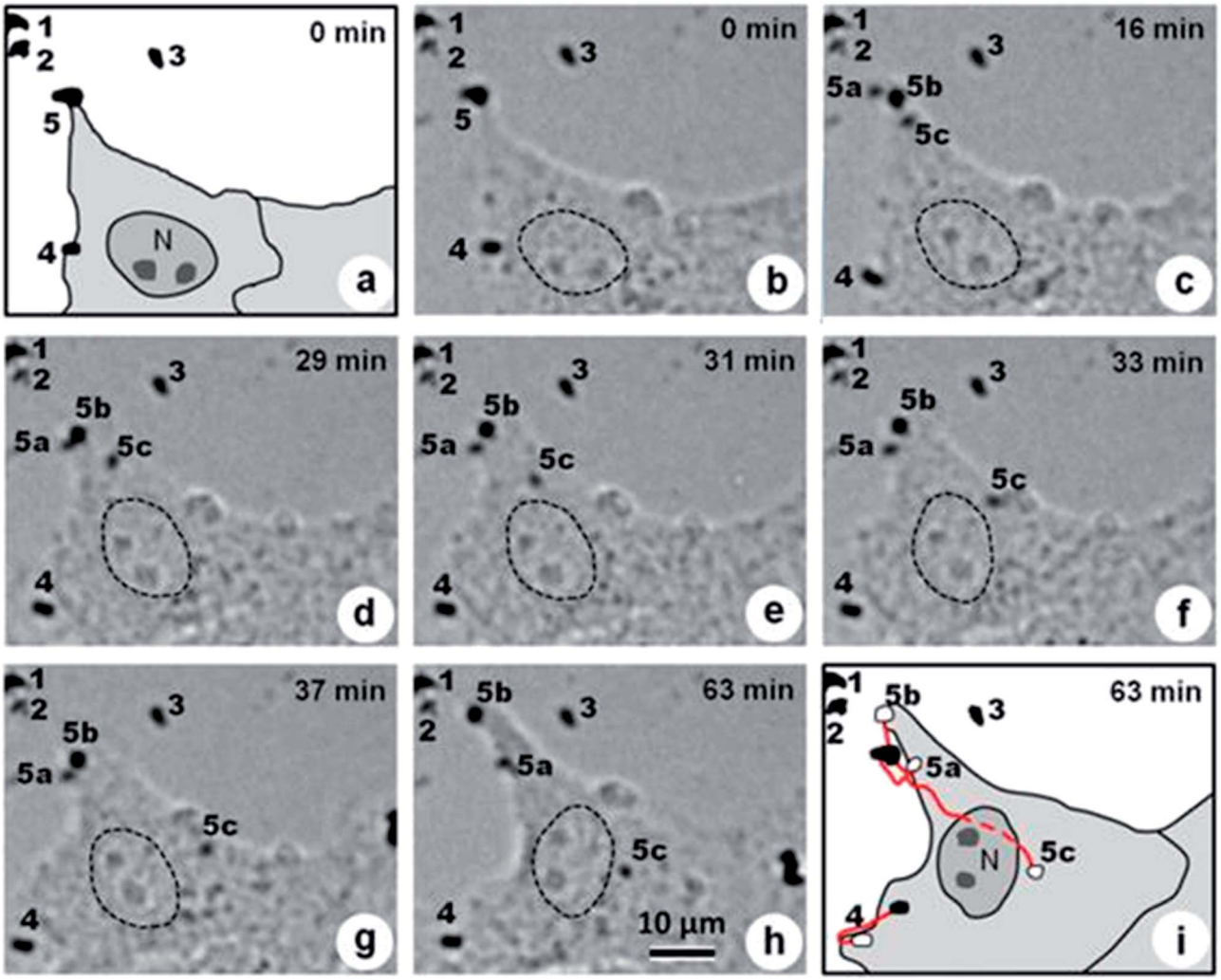

Fig. 7 Schemes and optical microscopy photographs representing the dynamics of interaction of Fe_7C_3@C NPs with living PK cells in the culture. Scheme of the cell and the positions of several agglomerates around it. Agglomerates are numbered from 1 to 5 (a). Successive photographs of the cell during living observations where the time elapsed after the beginning of the experiment is indicated in the right top corner of each photo. In the course of the experiment, the agglomerates 1, 2, and 3 remained motionless on the surface of the glass, while cluster number 5 after contact with the cell became divided into three separate agglomerates 5a, 5b, and 5c, agglomerate numbers 4, 5a, 5b remained associated with the cell membrane and moved with it, and cluster 5c became absorbed by the cell and moved quickly into it (b–h). The scheme shows the morphology of the cell and positions of the aggregates 4, 5a–c (white spots) after 63 minutes from the start of observation. The initial positions of the various agglomerates are shown by black spots. During the experiment, the cell nucleus is rotated clockwise and at the end of the experiment it reaches the position intersecting with the trajectory of the agglomerate 5c (i). Note that the cluster moves along the right side of the nucleus and never under, over or inside it. (see the ESI video recording 1†).

amount was found to be $0.3 \pm 0.11\%$, 72 h later it reached $1.3 \pm 0.56\%$, while in the cells with the added MNPs at a concentration of 20 μg ml^{-1} it comprised only $0.4 \pm 0.19\%$.

4 Discussion

Several critical reviews devoted to studies of properties of different types of magnetic NPs[6,16,27] have emphasized that the carbon-coated magnetic NPs of Fe, Co, Ni and iron carbides must possess a number of advantages in potential biomedical applications, as compared to the FePt alloy, and γ-Fe_2O_3, and Fe_3O_4 oxide NPs. It is considered that the carbon coating prevents aggregation of metal or carbide cores, preserving their single-domain structure and therefore consistency of the superparamagnetic nature of the particles. However, the widespread use of carbon-coated superparamagnetic NPs in biomedicine, until recently, was hampered by the fact that the existing methods for the synthesis of these particles are often characterized by low yields of the desired product. Another inconvenience is an incomplete carbon coating of individual NPs during their synthesis leading to the presence in the products of a certain percentage of pure metals with possible high toxicity.[40] Taking into account these observations, the review[16] stated that the synthesis of individual dispersed NPs having carbon coatings as well as control of the quality of these coatings are still unsolved problems.

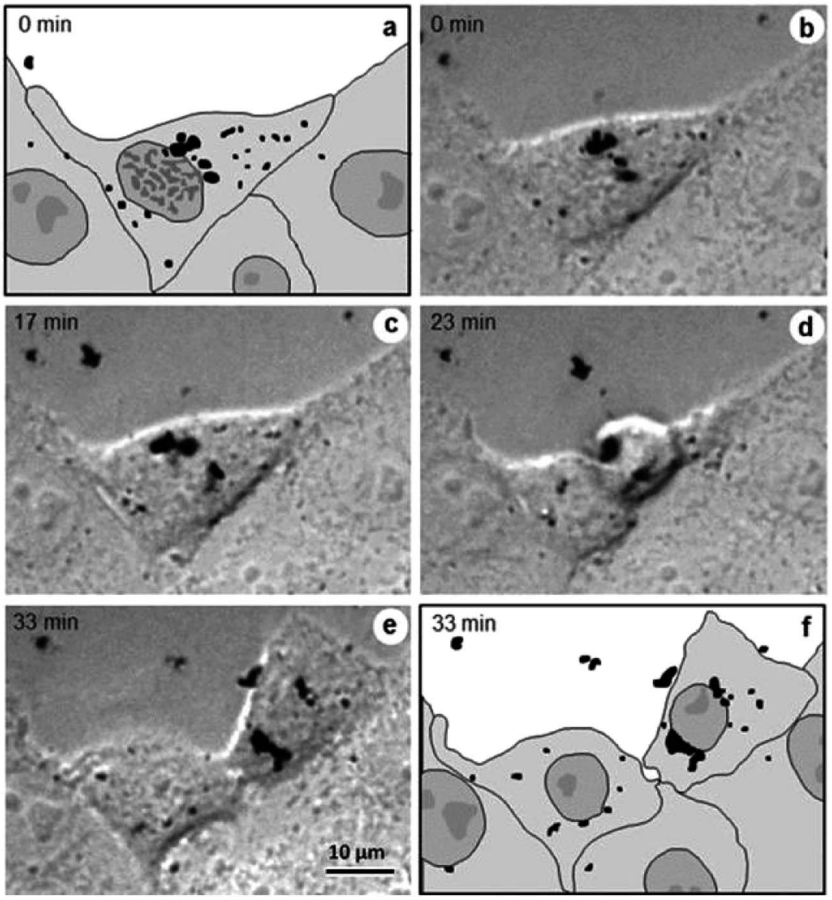

Fig. 8 Photographs of mitotic division in the PK cell with agglomerates of Fe_7C_3@C NPs. The scheme of the cell at the end of prophase of mitosis. Fe_7C_3@C agglomerates are shown in black, cytoplasm in light-grey, nucleus in grey, nucleolus and chromosomes (inside the nucleus of the central mitotic cell) in dark grey color and area free from cells in white (a). Successive photographs of cells during living observations, time elapsed after the beginning of the experiment is indicated in the left top corner of each photo. During the experiment agglomerates moved actively into the cell and finally turned to be unequally distributed between two daughter cells (b–e). The scheme of two daughter cells after the end of cell division (f), see the ESI video recording 2†.

The present study shows that the development of methods for synthesis of carbon-coated magnetic NPs based on pressure and temperature induced transformations of organometallic compounds, yielding superparamagnetic NPs comprising nearly 100% of the content of carbon-coated NPs, can give a possible solution to these problems. The existence of a clear dependence of the main characteristics of the produced carbide NPs on pressure, temperature parameters and time of isothermal treatment of the organometallic compound provides a reliable method for synthesis of nanomaterials with desired properties.

In the first step of the present study, the main controllable parameters of the synthesized material were the average size of the inner part of NPs, and the size of the carbide cores, which ensured their superparamagnetic properties. The methods of magnetic and fractional separation by sedimentation of Fe_7C_3@C NPs from the products of ferrocene transformation proposed in the present work allow obtaining pure fractions of encapsulated NPs with almost any desired size distribution.

Except the size and shape, the most important factor which defines the nature of the interaction of the nano-system with a biological object is the surface structure of the NPs, which affects the charge state, adsorption characteristics and other properties of the surface.[41] It is known that the surfaces of many carbon nanomaterials, such as fullerenes, carbon nanotubes, polyhedral and carbon onions are hydrophobic, which presents a big obstacle to their direct use for biomedical applications.[42] However, the grafting of various hydrophilic groups (such as COOH, OH, NH_2, … *etc.*) to the surface of these carbon materials can lead to modified NPs being able to produce sufficiently stable aqueous suspensions suitable for use in biomedical applications.[42] As already noted, in the case of carbon-encapsulated Fe_7C_3@C NPs, the outer layers of carbon shells produced directly in a high-pressure device, contain some hydrogen, and can be considered as hydrogen-terminated surfaces.

Moreover, when hydrogen peroxide, which is a mild oxidant, is used for partial deagglomeration of a related carbon matrix of the primary product of HPHTT of ferrocene, the surface modification of the encapsulated NPs occurs as a side process. This results in appearance on the surface of NPs of numerous oxygen-containing functional groups such as OH, C=O, COOH,

detected by the XPS method, which increase hydrophilicity of the NPs making them suitable for aqueous dispersibility. For this reason, the aqueous suspensions of our Fe_7C_3@C NPs are sufficiently stable.

In general, the study of the interaction of NPs with biological profiles at their various levels presents an extremely complex and multifaceted task. Even at the "simplest" cellular level, as in this work, the analysis of the processes of interaction of NPs with the cells involves the identification of ways to boost penetration into cells, studies of the distribution and the nature of the interaction of NPs with the various elements of the internal cell structure, and definition of the kinetic characteristics of the processes of endocytosis and exocytosis. From a biological point of view, important characteristics of the interaction are cytotoxicity, genotoxicity, oxidative stress and inflammatory effects resulting from the presence of the NPs in the biological system.[43] Currently, the penetration of extracellular materials into the cell was studied in sufficient detail.[44–46] Qualitatively, they can be divided into three main categories: diffusion (passive and active), pinocytosis and phagocytosis. The mechanism of passive diffusion involves the possibility of overcoming the cell membrane by individual atoms and small molecules due to the concentration gradient of the diffusing substance between the environment and the cytoplasm. Active diffusion uses the energy of ATP for transport of molecules and ions against the concentration gradient. Various options of pinocytosis provide the possibility for passage of external objects with the size ranging from a few up to hundreds of nanometers into the cell. Macropinocytosis and phagocytosis are the primary mechanisms for penetration into the cell of larger objects that can reach the size of several microns.

Our TEM investigations show that the penetration of Fe_7C_3@C NPs into the cell, as a rule, is carried out in the form of large, but rather weakly bound NP agglomerates. The formation of these agglomerates occurs on the outer surface of the cell membrane due to agglomeration of smaller clusters existing in extracellular solution (Fig. 6c). Part of large agglomerates may be formed in the volume of the culture medium or on the substrate surface free from cells. Given that the Fe_7C_3@C NPs penetrate into the cell with the extracellular fluid and that the characteristic size of the endocytotic vesicles is ~500 nm, we can assume that the macropinocytosis is the main mechanism of Fe_7C_3@C NP penetration into the studied cells. Membrane ruffling, being characteristic of this internalization pathway and shown in Fig. 6b, serves as a further confirmation of this hypothesis. However, since we observed sometimes in the cells significantly smaller agglomerates (Fig. 6c), we cannot exclude the possibility of the existence of other mechanisms of penetration of Fe_7C_3@C NPs into the studied cells. Note that the penetration of Fe_7C_3@C NPs into the PK cells is reminiscent of the penetration of nanodiamonds coated with polyethylenimine (ND–PEI) into the cells.[47] According to this report,[47] ND–PEI NPs can be also accumulated on the membrane in the form of "dynamic aggregates" having a critical size of ~500 nm and become finally absorbed by the cells through the mechanism of macropinocytosis. These "dynamical aggregates", defined as aggregates of nanoparticles with weak attractive interactions allowing changes in the shape,[47] present to the cell membrane a large surface of interaction at the early stages of internalization that may favor macropinocytosis. Interestingly, in the studies of internalization of unfunctionalized (ND) and acid-functionalized (ND–COOH) detonation nanodiamonds,[50] it was also noted that the characteristic dimensions of the aggregates of nanoparticles observed in the cytoplasm is ~500 nm. The authors[48] have found that the nanodiamonds, both with and without surface modification by an acid or a base, are biocompatible with a variety of cells of different origins including neuroblastoma, macrophage, keratinocyte and PC-12 cells. The comparison of our experiments with work carried out with nanodiamonds (ND)[44] shows that the rate of Fe_7C_3@C NP penetration into the cells is generally comparable with that for the ND.[47] We found that the first step of the uptake (15 to 120 min) approximately follows a linear behavior with time (Table 1), however, next 48 h of this behavior is exponential, with an estimated characteristic uptake half-life of 2.5 h. This measurement is compatible with the 2.6 h uptake half-life observed for NDs.[47] The characteristics of movement of absorbed agglomerates of Fe_7C_3@C NPs suggest a possible participation of cytoskeletal units, particularly the system of microtubules, in their intracellular transport. In our case, we observed a centripetal almost rectilinear motion of Fe_7C_3@C NP agglomerates with the rate of up to 1.6 microns per minute. This suggests the participation of the dynein-associated cellular transport systems in moving the NP clusters, enclosed in a membrane envelope.

The presence of intracellular agglomerates of Fe_7C_3@C NPs has no significant effect on the cell morphology. The ultrastructure of all organelles is not different from control cells. Cells pass mitosis without apparent delays and the Fe_7C_3@C NP agglomerates become randomly distributed between daughter cells. We did not find even more remoted consequences of Fe_7C_3@C NP action on cell morphology and physiology. Even after 10 days of culturing cells with Fe_7C_3@C NPs, no increase in the cell death was found. However, a comprehensive and extensive investigation, with practical dosages that are adequate and suitable for an *in vivo* study, is urgently needed for future clinical applications.

5 Conclusions

We have successfully synthesized superparamagnetic carbon-encapsulated iron carbide NPs by HPHTT of ferrocene with nearly 100% efficiency. This method shows advantages compared to the existing synthetic protocols because it allows control of the main physical characteristics of Fe_7C_3@C NPs. The developed purification and separation protocol in this work allows preparation of sufficiently uniform quasi-spherical NPs with the given average size.

Summarizing the results of all three cytotoxicity assays we can conclude that Fe_7C_3@C NPs under chosen experimental conditions display high efficiency of cellular uptake and do not affect cytophysiological parameters of *in vitro* cultured cells. The high efficiency of Fe_7C_3@C NP internalization by the studied PK cells is a key parameter for evaluation of Fe_7C_3@C NPs as

potential drug delivery vectors. The relatively large size of our Fe_7C_3@C agglomerates (500 nm) can reduce the chance for them to be excreted from an organism with the urine.[50] Macropinocytosis is the main mechanism of Fe_7C_3@C NP penetration into the studied PK cells. We have also demonstrated that the relatively high concentrations of Fe_7C_3@C NPs in culture media did not affect the time course of mitosis, progression through the synthetic phase of the cell cycle or overall proliferative activity of the cells. The previous conclusions concerning low toxicity and high chemical stability of nanoparticles with carbon-modified surfaces[16,49] were confirmed.

The next step in the continuation of this work will be to study the specific mechanism of NP movement in the cells and the action of the magnetic field on this behavior of NPs.

Acknowledgements

This work was supported by the Russian Foundation for Basic Research (Grants 12-03-00787, 12-04-00488, 13-04-00885) and the Moscow State University Development Program PNR 5.13. We thank Pierre-Yves Sizaret for help in the fraction analysis and Jean Yves Tartu for technical assistance in the mechanical adaptation of the microscopy table for living observations. Our data were obtained with the assistance of the RIO Electron Microscopy Facility of François Rabelais University and CHRU de Tours.

References

1 S. P. Gubin, Y. A. Koksharov, G. B. Khomutov and G. Yu Yurkov, *Russ. Chem. Rev.*, 2005, **74**, 489–520.
2 T. Neuberger, B. Sehopf, H. Hofmann, M. Hofmann and B. von Rechenberg, *J. Magn. Magn. Mater.*, 2005, **293**, 483–496.
3 Q. A. Pankhurst, J. Connolly, S. K. Jones and J. Dobson, *J. Phys. D: Appl. Phys.*, 2003, **36**, R167–R181.
4 M. Hofmann-Amtenbrink, B. von Rechenberg and H. Hofmann. *Nanostructured Materials for Biomedical Applications*, ed. M. C. Tan, Research Signpost, 2009, pp. 119–143.
5 M. Mahmudi, S. Sant, B. Wang, S. Laurent and T. Sen, *Adv. Drug Delivery Rev.*, 2011, **63**, 24–46.
6 A. V. Bychkova, O. N. Sorokina, M. A. Rosenfeld and A. L. Kovarski, *Russ. Chem. Rev.*, 2012, **81**, 1026–1050.
7 J. L. Gilmore, X. Yi, L. Quan and A. V. Kabanov, *Journal of NeuroImmune Pharmacology*, 2008, **3**, 83–94.
8 T. J. Deerinck, *Toxicol. Pathol.*, 2008, **36**, 112–116.
9 S. J. Son, X. Bai and S. B. Lee, *Drug Discovery Today*, 2007, **12**, 650–656.
10 R. Duncan and F. Spreafico, *Clin. Pharmacokinet.*, 1994, **27**, 290–306.
11 B. J. Boyd, *Expert Opin. Drug Delivery*, 2008, **5**, 69–85.
12 R. Duncan, *Biochem. Soc. Trans.*, 2007, **35**, 56–60.
13 K. Holt, *Philos. Trans. R. Soc., A*, 2007, **365**, 2845–2861.
14 A. M. Schrand, S. A. C. Hens and O. A. Shenderova, *Crit. Rev. Solid State Mater. Sci.*, 2009, **34**, 18–74.
15 D. L. Huber, *Small*, 2005, **1**, 482–501.
16 A. H. Lu, E. L. Salabas and F. Schuth, *Angew. Chem., Int. Ed.*, 2007, **46**, 1222–1244.
17 P. C. Eklund, X. X. Bi. Quartery progress report, Center for Applied Energy Research, University of Kentucky, Lexington, 1992.
18 J. Jiao, S. Seraphin, X. Wang and J. C. Withers, *J. Appl. Phys.*, 1996, **80**, 103–108.
19 L. Ning, L. Xiaojie, W. Xiaohong, Y. Honghao, Z. Chengjiao and W. Haitao, *Carbon*, 2010, **48**, 3858–3863.
20 Z. Schnepp, S. C. Wimbuch, M. Antonietti and C. Girdano, *Chem. Mater.*, 2010, **22**, 5340–5344.
21 A. K. Gupta and S. Wells, *IEEE Transactions on NanoBioscience*, 2004, **3**, 66–73.
22 L. Xu, M.-J. Kim, K.-D. Kim, Y.-H. Choa and H.-T. Kim, *Colloids Surf., A*, 2009, **350**, 8–12.
23 G. B. Shan, J. M. Xing, M. F. Luo, H. Z. Liu and J. Y. Chen, *Biotechnol. Lett.*, 2003, **25**, 1977–1981.
24 S. Prijie and G. Sersa, *Radiol. Oncol.*, 2011, **45**, 1–16.
25 C. C. Berry, S. Wells, S. Charles and A. S. G. Curtis, *Biomaterials*, 2003, **24**, 4551–4557.
26 M. Uo, K. Tamura, Y. Sato, A. Yokoyama, F. Watari, Y. Totsuka and K. Tohji, *Small*, 2005, **1**, 816–819.
27 J. K. Park, J. Jung, P. Subramaniam, B. P. Shah, Ch. Kim, J. K. Lee, J.-H. Cho, Ch. Lee and K.-B. Lee, *Small*, 2011, **7**, 1647–1652.
28 A. Tsuzuki, S. Sago, S.-I. Hirano and S. Naka, *J. Mater. Sci.*, 1984, **19**, 2513–2518.
29 V. Davydov, A. Rakhmanina, H. Allouchi, C. Autret, P. Limelette and V. Agafonov, *Fullerenes, Nanotubes, Carbon Nanostruct.*, 2012, **20**, 451–454.
30 R. H. Bagramov, V. D. Blank, N. V. Serebryanaya, G. A. Dubitsky, E. V. Tatyanin and V. V. Aksenenkov, *Fullerenes, Nanotubes, Carbon Nanostruct.*, 2012, **20**, 41–48.
31 L. G. Khvostantsev, L. F. Vereshchagin and A. P. Novikov, *High Temp. – High Pressures*, 1977, **9**, 637–639.
32 C. A. Schneider, W. S. Rasband and K. W. Eliceiri, *Nat. Methods*, 2012, **9**, 671–675.
33 M. W. Freeman, A. Arrot and J. H. L. Watson, *J. Appl. Phys.*, 1960, **31**, 404–405.
34 A. Edelstein, N. Amodaj, K. Hoover, R. Vale and N. Stuurman, *Current Protocols in Molecular Biology*, 2010, 14201–142017.
35 F. H. Hebstein and J. A. Snyman, *Inorg. Chem.*, 1964, **3**, 894–896.
36 D. Ugarte, *Carbon*, 1995, **33**, 989–993.
37 C. P. Bean and J. D. Livingston, *J. Appl. Phys.*, 1959, **30**, 120–129.
38 R. Sappey, E. Vincent, N. Hadacek, F. Chaput, J. P. Boilot and D. Zins, *J. Phys. Chem. B*, 1997, **56**, 14551–14559.
39 M. F. , Hansen and S. J. Morup, *J. Magn. Magn. Mater.*, 1999, **203**, 214–216.
40 J. Geng, D. A. Jefferson and B. F. G. Johnson, *Chem. Commun.*, 2004, 2442–2443.
41 G. Oberdorster, V. Stone and K. Donaldson, *Nanotoxicology*, 2007, **1**, 2–25.
42 H.-W. Yang, M.-Y. Hua, H.-L. Liu, C.-Y. Huang and K.-Ch. Wei, *Nanotechnol., Sci. Appl.*, 2012, **5**, 73–86.

43 J. Boczkowski and P. Hoet, *Nanototoxicology*, 2010, **4**, 1–14.
44 S. D. Conner and S. L. Schmid, *Nature*, 2003, **422**, 37–44.
45 H. Hillaireau and P. Couvreur, *Cell. Mol. Life Sci.*, 2009, **66**, 2873–2896.
46 A. Panariti, G. Miserocchi and I. Rivolta, *Nanotechnol., Sci. Appl.*, 2012, **5**, 87–100.
47 C. Alhaddad, A. Durieu, G. Dantelle, E. Le Cam, C. Malvy, F. Treussart and J.-R. Bertrand, *PLoS One*, 2012, **7**, 1–8.
48 A. M. Schrand, H. Huang, C. Carlson, J. J. Schlager, E. Osawa, S. M. Hussain and L. J. Dai, *J. Phys. Chem. B*, 2007, **111**, 2–7.
49 S. I. Nikitenko, Y. Koltypin, O. Palchik, I. Felner, X. N. Xu and A. Gedanken, *Angew. Chem., Int. Ed.*, 2001, **40**, 4447–4449.
50 C. Boyer, M. R. Whittaker, V. Bulmus, J. Liu and T. P. Davis, *NPG Asia Mater.*, 2010, **2**, 23–30.